Journal of Research in Health Sciences
ISSN: 2228-7809 | https://jrhsjournal.com

Structural and Kinetic Insights into Amyloid-β (1–40) Aggregation and Fibril Formation

Dr. Alexander Hughes[1]*, Dr. Emily Carter[1], Dr. James Whitmore[2], Dr. Sophie Bennett[2], Dr. Daniel Clarke[3], Dr. Olivia Harris[3]
[1]University College London Hospitals NHS Foundation Trust, London, United Kingdom
[2]Imperial College Healthcare NHS Trust, London, United Kingdom
[3]University of Oxford Medical Sciences Division, Oxford, United Kingdom

ABSTRACT

The aggregation kinetics of Aβ1-40 peptide was characterized using a synergistic approach by a combination of nuclear magnetic resonance, thioflavin-T fluorescence, transmission electron microscopy and dynamic light scattering. A major finding is the experimental detection of high molecular weight oligomers (HMWO) that converts into fibrils nuclei. Our observations are consistent with a mechanism of Aβ1-40 fibrillogenesis that includes the following key steps: i) slow formation of HMWO (Rh~20nm); ii) conversion of the HMWO into more compact Rh~10nm fibrils nuclei; iii) fast formation of additional fibrils nuclei through fibril surface catalysed processes; and iv) growth of fibrils by addition of soluble Aβ species. Moreover, NMR diffusion experiments show that at 37°C soluble Aβ1-40 remains intrinsically disordered and mostly in monomeric form despite evidences of the presence of dimers and/or other small oligomers. A mathematical model is proposed to simulate the aggregation kinetics of Aβ1-40.

Keywords: amyloid, nucleation, amyloid-β peptide, alzheimer's disease, aggregation kinetics, amyloid-β peptide oligomers, Aβ1-40

1. Introduction

The denaturation and aggregation of proteins and peptides, resulting in the loss of their structural and functional properties and the formation of amyloid-like fibrous deposits, are associated with more than 20 diseases, like Huntington's, Parkinson's or Alzheimer's disease (AD). Intriguingly, the site of deposition and the pathologies associated may diverge significantly due to, for example, a single amino acid mutation. The main component of amyloid aggregates found in the brains of Alzheimer's patients are the β-amyloids peptides. These peptides are produced by the two-step cleavage of the amyloid precursor protein (APP) by β- and γ-secretases[1]. The most prevalent form is Aβ1-40, followed by Aβ1-42, and other less prevalent N-terminal truncated or post-synthetically modified forms, such as Aβ2-x and AβpE3-x.

The amyloidogenic aggregates, independent of the source protein, show common features which enable their distinction from amorphous precipitates by several methods. Congo red staining, thioflavin-T fluorescence, ultra-structural analysis, circular dichroism and X-ray diffraction are among the most used[2]. A major breakthrough was the production of an antibody that specifically recognizes soluble oligomers of many amyloidogenic proteins and peptides[3], which indicates that they definitely share a common structure.

High-resolution techniques used for the determination of the structure of biomolecules, such as X-ray crystallography and nuclear magnetic resonance (NMR), are less suitable for analysis of high molecular weight amyloid arrangements. Thus, the self-assembly mechanism at the molecular level has remained elusive. In this context, the analysis of the kinetics of protein aggregation, which can be followed by a plethora of biophysical and

biochemical methods [4], has become a valuable tool in deciphering the mechanistic models. The problem is that typically the progression of protein aggregation follows a sigmoidal curve that can be fitted by many mathematical functions. The topic has been the subject of comprehensive reviews [4, 5].

Different approaches have been used to predict the protein polymerization process, ranging from atomistic simulations [6-8] to mesoscopic mass actions equations (for a review see ref. [4]). Thermodynamically, the process has been described at different levels of detail [9-11]. An increase in the model's complexity can lead to over-parametrization and make the simulations too difficult, whilst oversimplification may weaken the theoretical foundations of the model. Probably, among the most used are the Ferrone model that postulated the presence of secondary events [12, 13]; the Finke–Watzky model based on nucleation followed by autocatalytic surface growth [14]; and the Knowles analytical equation of the mechanistic model that combines primary nucleation, secondary nucleation, fibril elongation and fibril fragmentation [15].

Despite the diversity of mathematical models available in the literature, it is believed that proteins polymerize through a common mechanistic model, consisting in a nucleation-dependent polymerization where the formation of nuclei from soluble proteins is slower than the elongation step. However, it was noticed that experimental data were sometimes not correctly predicted by this simple two-step mechanism. Thus, secondary nucleation processes were proposed, in which the two most popular are fibril fragmentation [2, 11, 15, 16], suggested to be involved in *β*2-microglobulin aggregation and prion propagation, and heterogeneous nucleation which was detected in the polymerization of insulin [17-20] and

amyloid-*β* peptide [21-23], and in the gelation of sickle cell hemoglobin at low concentrations [10].

The aggregation of amyloid-*β* peptides remains particularly elusive. Knowles and colleagues developed a widely accepted model for the aggregation of Aβ1-42 based on the presence of two species, monomers and fibrils [22]. The authors could not fit this model to the kinetic curves of Aβ1-40 without major assumptions regarding the dependence of secondary nucleation events on the concentration of monomers [23]. On the other hand, Lomakin and co-workers [21] and Luchinat and co-workers [24], among others, provided evidences for the conversion of Aβ1-40 oligomers into fibrils nuclei. NMR techniques have been used to identify and characterize the formation of Aβ oligomers in solution and in the presence of lipid membranes [25-27]. Very recently, Knowles and colleagues also brought up evidence of the presence of a population of Aβ1-42 oligomers during the initial stages of aggregation [28]. Thus, the mechanism of aggregation of amyloid-*β* peptides is more complex than previously thought, which prompted us to investigate the aggregation of Aβ1-40 using a combination of complementary experimental techniques that enable us to observe the shape/mass variation of Aβ1-40 species in the early stages.

2. Materials and Methods

2.1. Reagents

Aβ peptides 17-40, 1-40 and 1-42 were purchased from Bachem (Switzerland) with HPLC determined sample purity of 91.6%, 93.7% and 96.7%, respectively. Aβ peptide solutions were prepared based on ref. [29]. Briefly, Aβ peptides were equilibrated at room

temperature for 30 minutes to allow complete defrosting and spun before opening the vial. To each sample, 500 µl of 1,1,1,3,3,3-Hexafluoro-2-propanol (HFIP) were added to complete disassemble pre-existing aggregates. Samples were incubated at room temperature overnight. HFIP was removed under a gentle flow of pure nitrogen gas and further dried with a vacuum concentrator to remove remaining traces. If samples were not clear after a single HFIP passage, the procedure was repeated, adding a brief homogenization step using a sonication bath. Dried peptide films were thoroughly resuspended in pure dimethyl sulfoxide (DMSO) and stored at -20˚C between measurements. All other reagents were of analytical grade.

2.2. NMR spectroscopy

All experiments were performed at 37 °C using a Bruker Avance III 600 MHz spectrometer.

1H-NMR Experiments. Samples for the 1D 1H-NMR experiments were prepared in deuterated buffer (TRIS-d11 50mM, EDTA-d16 1mM, pH 7.4) with a peptide concentration of 60µM. 25µM of 3-(Trimethylsilyl)propionic-2,2,3,3-d4 acid sodium salt (TSP) was used as internal standard. Samples are prepared at room temperature and maintained at 37 °C. The aggregation process was monitored by following the ^{1}H signal intensities of the peptide (relative to the signal intensity of the internal standard TSP) in 1D spectra over time. ^{1}H spectra were acquired with 256 transients and 2 s recycle delay. The excitation sculpting scheme was employed to suppress residual H_2O signal[30].

Diffusion experiments. Samples for DOSY experiments were prepared similarly as above: deuterated buffer (TRIS-d_{11} 50mM, EDTA-d_{16} 1mM, pH 7.4) with a peptide concentration of

60µM. During the aggregation process DOSY experiments were measured at 37 °C and performed employing an array of 32 spectra for each experiment (128 or 256 transients each, with a 1 s recycle delay), and varying the gradient strength between 2% and 95%. The lengths of and delays between the gradient pulses were optimized for each sample. Data fitting and diffusion coefficients determination were performed with the T1/T2 Relaxation module available in the Bruker TopSpin software.

The radius of gyration (R_g) of reference aprotinin was computed with model coordinates PDB 4PTI[31] using the program HYDROPRO [32]. The hydrodynamic radius (R_h) of a globular protein such as the reference can be predicted by the relationship $R_g = \sqrt{3/5}R_h$.

Diffusion coefficients are inversely proportional to the hydrodynamic radius as shown by the Stokes-Einstein equation:

$$D = \frac{k_B T}{6\pi\eta R_h} \quad (1)$$

Thus, for Aβ peptides and reference in the same solution,

$$R_h^{A\beta} = \frac{D^{ref}}{D^{A\beta}} R_h^{ref} \quad (2)$$

2.3. Dynamic Light Scattering (DLS)

Aβ1-40 2 mM stock in DMSO was diluted to 50 µM in 10 mM sodium phosphate buffer pH 7.4. Samples were centrifuged for 15 minutes at 5000x g to remove pre-formed aggregates. DLS measurements were performed at 25°C using an ALV/DLS/ SLS-5000F instrument equipped with a SP-86 goniometer system (ALV-GmbH, Langen, Germany) and a CW diode-pumped Nd:YAG solid-state Compass-DPSS laser with a symmetrizer (Coherent Inc., Santa

Clara, CA). The laser operates at 532 nm with an output power of 400 mW. The intensity scale was calibrated against scattering from toluene. Measurements were made at a scattering angle 90° to the incident beam for 5-10 min, for time points 0h, 2h, 4h, 6h and 8h. Data were analyzed with ALV Correlator Software (version 3.0).

2.4. Thioflavin-T (ThT) amyloid formation kinetics

Amyloid fluorescent dye Thioflavin-T (ThT) was used to follow amyloid kinetics. ThT stock solution was freshly prepared for each set of measurements at a concentration of 3 mM in ultrapure water (concentration was determined spectrophotometrically at 411 nm, $\varepsilon = 2.2 \cdot 10^4\ M^{-1}\ cm^{-1}$). Aβ peptides were diluted to the final concentration from the working DMSO stocks in 20 mM sodium phosphate buffer at pH 7.4. The measured ThT concentration was 30 µM. Measurements were made at 37°C at quiescent conditions with a plate fluorimeter FluorDia T70 (Otsuka Electronics, Japan) using ThT excitation and emission filters (440 nm and 480 nm, respectively). Triplicate measurements were performed in 96-well plates (total volume of 300 µl) and averaged. Each well was sealed with 30 ul paraffin oil to avoid evaporation.

2.5. Transmission electron microscopy

Aliquots (10 µl) of Aβ1-40 and Aβ17-40 mature fibril solutions were adsorbed onto carbon-coated Formvar 300-mesh nickel grids (Electron Microscope Sciences, USA). The grids were washed and stained with 2% (w/v) uranyl acetate. The samples were viewed with a TEM JEOL JEM-1400 microscope (JEOL Ltd., Tokyo, Japan) at 120 kV.

3. Results and Discussion

Hydrodynamic radius of proteins and peptides, namely of amyloid beta fragments, are remarkably well fitted to the molecular mass (or the number of chain residues) by scaling laws[33-35]. Estimation of the scaling factor provides a framework that can be used to analyse the conformational properties [33-35] and/or the oligomerization state [34] of proteins and peptides underscoring the usefulness of analysing more than one amyloid beta fragment. Thus, in addition to Aβ1-40, the biological relevant Aβ17-40 peptide was investigated by NMR techniques. Aβ17-40, also called P3 peptide, results from the α- and γ-secretase cleavage of the amyloid precursor protein (APP) and is, similarly to the full length peptides, a major constituent of diffuse plaques observed in Alzheimer's disease (AD) brains and pre-amyloid plaques in people affected by Down's syndrome. [36]

Aggregation kinetics of Aβ1-40 and Aβ17-40 peptides was followed by NMR. Simple 1D ^{1}H - NMR experiments were acquired, and a decay in the intensities of the proton signals of the peptide over time was observed. The presence of new peaks was not detected. Although exchange processes could also provide signal broadening [37, 38], these observations strongly pointed to the conversion of the peptide monomer or small sized oligomers (NMR visible species) into large sized oligomeric species (species whose NMR signals are broadened beyond detection, i.e. NMR-invisible species). Thus, monitoring the reduction of the proton signal intensity reduction over time can be exploited to measure the aggregation kinetics (Fig. 1).

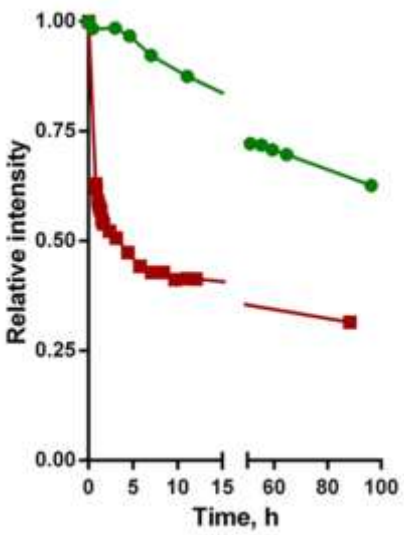

Fig. 1. Aggregation of Aβ1-40 (green) and Aβ17-40 (red) followed by NMR. Decay of the relative ^{1}H -NMR signal intensity of the soluble species.

The aggregation behavior of the two Aβ peptides was remarkably different. Aβ1-40 showed the expected nucleation polymerization behaviour, observed by other investigators [23, 24], while the concentration of Aβ17-40 soluble species decays exponentially with time, which point to a protective role of the *N*-terminal region against aggregation. Moreover, diffusion ordered spectroscopy (DOSY) experiments provided information about the size/shape of the visible species during the time course of the aggregation process. Interestingly, the diffusion coefficients, and thus the average size of these species (hydrodynamic radius calculated using equation 2), remained nearly constant within the experimental uncertainty for both Aβ1-40 and Aβ17-40 peptides (Table 1).

Table 1. Diffusion coefficients and corresponding hydrodynamic radius determined by NMR at 37°C

Compound	Diffusion coefficient (m^2/s) [a]	MW (Da)	R_h (Å)
Aprotinin	$1.88 \cdot 10^{-10}$	6500	15.8
Aβ17-40	$(1.99 \pm 0.05) \cdot 10^{-10}$	2393	14.9
Aβ1-40	$(1.49 \pm 0.05) \cdot 10^{-10}$	4330	19.9

[a] For Aβ peptides averaged values are displayed.

Several researchers have found that hydrodynamic radius of proteins and peptides with N_R residues are well fitted to the scaling law:

$$R_h = R_o {N_R}^{\nu} \quad (3)$$

The scaling factor ν was empirically determined to be 0.29 for native folded proteins and 0.57 for highly denatured peptides and proteins by Smith and co-workers [35]; the authors measured hydrodynamic radii by pulse field gradient PFG-NMR techniques. Damaschun *et al.* reported $\nu = 0.5 \pm 0.02$ obtained from proteins denatured in 6 M guanidine hydrochloride [33]. Danielsson and colleagues studied the hydrodynamic properties of Aβ fragments at 25°C, also by PFG-NMR, and found $\nu = 0.415$ [34]. The exponent lies below the exponent for the fully denatured state but above the exponent for the native. The authors concluded that there is some residual structure in the longer Aβ fragments at 25°C.

Despite the fact we have only collected data for two Aβ peptides, it is interesting to observe they correlate by a scaling factor $\nu = 0.57$ which strongly suggests that these peptides remain fully disordered at 37°C. Furthermore, the scaling data for disordered proteins collected by Smith *et al.* [35] was used to estimate the expected number of residues (N_R) of

peptides whose hydrodynamic radii matches the ones measured for Aβ1-40 and Aβ17-40 (Table 1). As can be observed in Figure 2, $R_h = 19.9$Å is expected for a peptide of 49 residues and $R_h = 14.9$Å for a peptide of 29 residues. The Aβ peptides are shorter than predicted even assuming that they are fully disordered which is an indication that there should be some degree of oligomerization at 37°C.

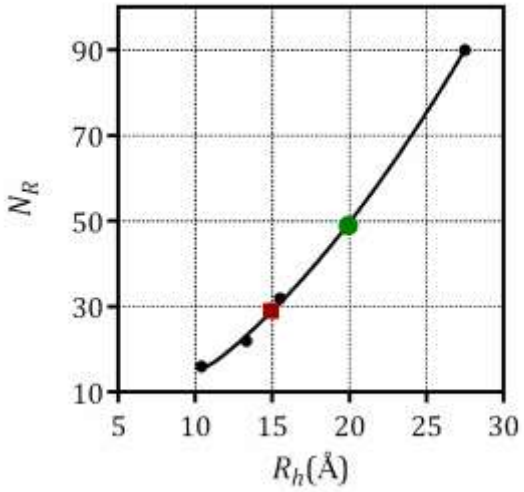

Fig. 2. Plot of the number of residues of highly denatured polypeptide chains versus the hydrodynamic radius. Black symbols are values reported by [35], green and red symbols denote the measured hydrodynamic radius of Aβ1-40 (green) and Aβ17-40 (red), respectively.

It is reasonable to assume that monomeric and dimeric peptides give the major contributions to the decay of the resonance intensity in the diffusion experiment of Aβ peptides [34]. If the chemical shifts of the monomer and the dimer are the same, the measured diffusion coefficient is the weighted mean value of the two diffusion coefficients [34] and

$$\frac{1}{(R_h)_{meas}} = f_{mon}\frac{1}{(R_h)_{mon}} + f_{dimer}\frac{1}{(R_h)_{dimer}} \quad (4)$$

Making use of the empirical correlation for unfolded peptides and proteins provided by Smith *et al.* [35] to estimate the hydrodynamic radius of the pure species yields an approximate mass fraction of monomers of nearly 65%, both for Aβ1-40 and Aβ17-40. Thus, there is a measurable degree of dimerization at physiological temperature (37°C) in contrast to what was observed at 25°C [34]. DOSY experiments are not expected to provide multimodal results in a mixture of monomer to tetramer Aβ species, however, dimers and tetramers of Aβ1-40 were already identified as major species in solution using ion mobility coupled with mass spectrometry[39] and photoinduced cross-linking [40].

Transmission electron microscopy (TEM) analysis of Aβ mature samples confirms that Aβ1-40 fibrils are longer and present in a smaller number than Aβ17-40 ones (Fig. 3). Moreover, Aβ17-40 fibrils show a propensity for lateral packing, while some Aβ1-40 fibrils exhibit twisting of two protofilaments.

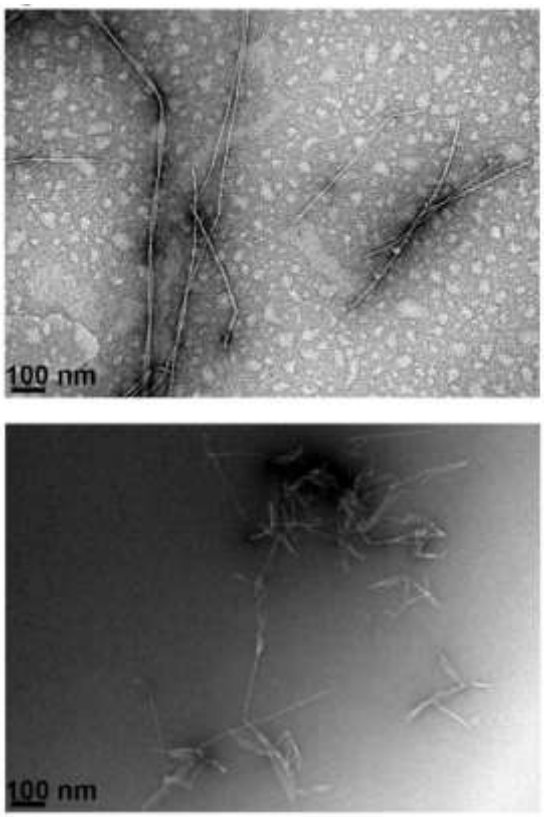

Fig. 3. TEM images of mature fibrils of Aβ1-40 (top) and Aβ17-40 (bottom).

The aggregation of Aβ1-40 was further monitored by dynamic light scattering (DLS), which enables the observation of aggregates (NMR-invisible species) since the scattering intensity is very dependent on the particle mass/size. The evolution of the particle size distribution with time is shown in Fig. 4. These data indicate that soluble Aβ1-40 do not nucleate directly into fibrils but go through a transient oligomeric state. When the oligomers reach a critical oligomeric size (HMWO with Rh ~20nm) they seem to irreversible convert to fibrils nuclei (Rh ~10nm). Fibrils grow by the addition of Aβ1-40 soluble species (which are no longer detected due to the much stronger scattering intensity of the large entities) at a rate of ~1.5nm/h in the used experimental conditions. As fibrils grow, the concentration of Aβ1-40 soluble species falls and no more HMWO formation occurs, achieving a separation in time

between the two processes, HMWO formation and fibril growth. A similar two-step model was already proposed by Luchinat's group [24] based on the analysis of the kinetic curves and not in the direct observation of these transient species. Lomakin and colleagues [21] studied the fibrillogenisis of Aβ1-40 in acidic conditions using quasi-elastic light-scattering spectroscopy and proposed that fibrils nuclei emerge from micelles and that, actually, nuclei are smaller.

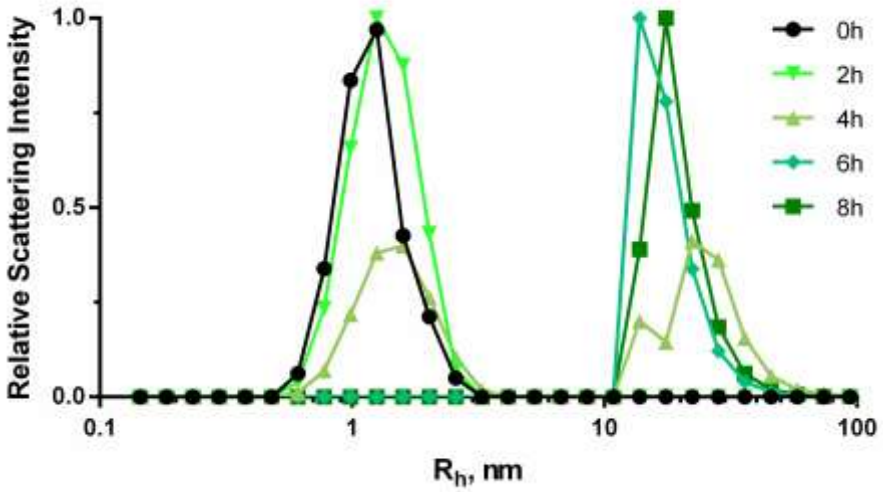

Fig. 4. Temporal evolution of Aβ1-40 hydrodynamic radius (Rh), followed by DLS.

The data in Fig.3 has two additional important features. The formation of the HMWO (Rh~20nm) is neither spontaneous nor occurs at constant rate (not detected at t= 2h but very visible at t= 4h). Secondly, the fibrils nuclei (Rh~10nm) outnumbered HMWO since the relative scattering signal of the soluble species disappeared once HMWO starts to convert into first nuclei. The most plausible explanation is that fibril nucleus are also formed by surface processes (secondary) which occur in a much shorter time scale than the primary

nucleation events. Fibril surface catalysed nucleation seems to produce directly compact fibril nucleus as large oligomers (Rh~20nm) cease to be detected.

The present results are in agreement with the conversion model illustrated in Fig. 5. The first step consists in the formation of HMWO and depends on the concentration of monomers (m_0). The second step corresponds to the structural conversion of HMWO into fibrils nuclei, which should not depend on the concentration of the soluble peptide. Then, the number of fibrils nuclei seems to rapidly increase probably due to heterogeneous nucleation.

For high monomer concentrations, the formation of HMWO becomes fast and the characteristic time for the formation of fibrils nuclei (t_{MN}^*) approximates the time of conversion of HMWO into nuclei (t_N^*), remaining independent of m_0 (phase I in Fig. 5).

For low concentrations of m_0, the HMWO formation kinetics (t_M^*) plays a role in the dynamics of the whole system. It is expected that the formation of HMWO occurs at nearly constant monomer concentration $m \sim m_0$, and most of the monomer is consumed in the fibril growth step. Moreover, if HMWO are formed by a step-wise addition of monomers, the average time of HMWO formation is $t_M^* \sim m_0^{-1}$, as it will be discussed later (phase II, in Fig. 5). In the unforeseen case that most of the monomer is consumed in the formation of HMWO, the reaction rate is $\sim m_0^2$ and $t_M^* \sim m_0^{-2}$(phase III in Fig. 5). If fibril growth is significantly faster than nucleation $t_{1/2}$, the characteristic half-time of reaction (that is, the is the time at which 50% of the protein is found in aggregated form), should maintain the same monomer dependence as t_{MN}^* (Fig. 5). Indeed, it was already observed for Aβ1-40 that this scaling exponent is highly dependent on the concentration, and it varies from −1.2 ± 0.2

at low protein concentrations (ca. 5 μM) to −0.2 ± 0.05 at higher protein concentrations (ca. 60 μM).[23]

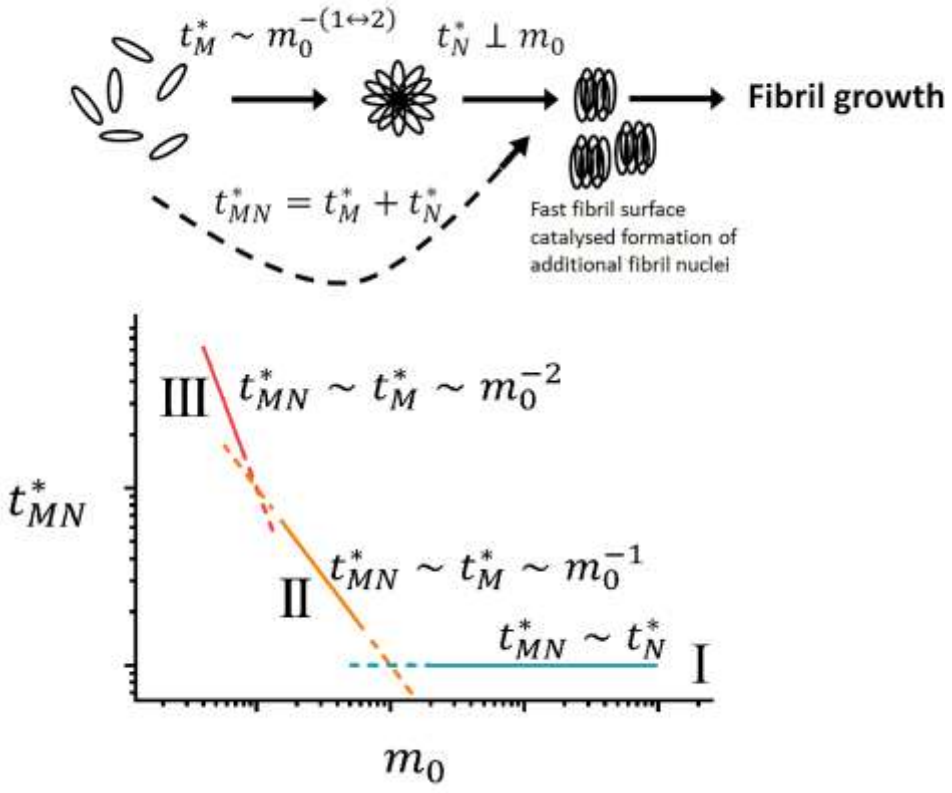

Fig. 5. Proposed two-step conversion model for Aβ1-40 aggregation (top) and characteristic fibril nucleation time dependence on the initial concentration of monomer (bottom).

If formation of HMWO is represented by a step-wise addition reaction of N monomers and the addition rates are considered constant $Km_0 = k_+ m_0 - k_-$ (m_0 being the initial monomer concentration), the concentration of HMWO $M(t)$ can be readily calculated by [41]:

$$\frac{M(t)}{M_\infty} = 1 - \sum_{i=1}^{N} \frac{(Km_0 t)^{i-1} e^{-Kt}}{(i-1)!} \quad (5)$$

The average time of HMWO formation is then $E(t) = N/Km_0$. In Fig. 6, $M(t)/M_\infty$ are presented for different N.

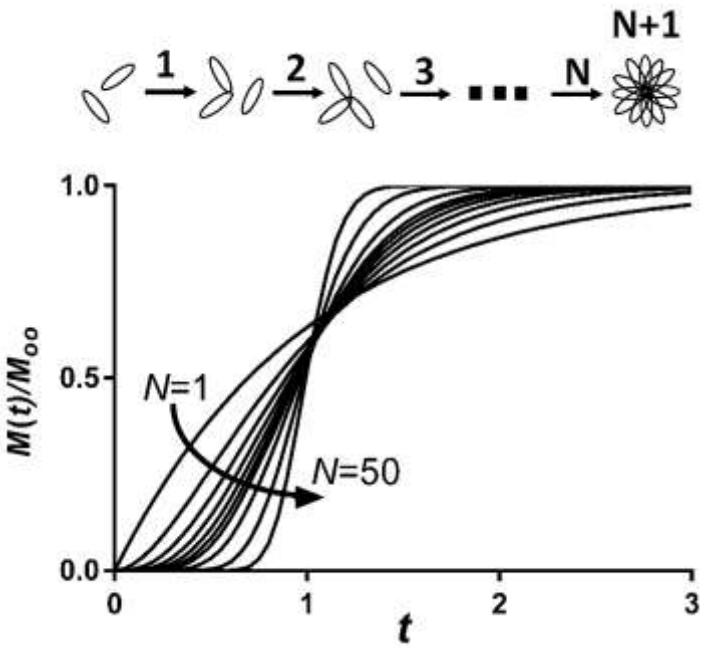

Fig. 6. $M(t)/M_\infty$ profiles for increasing number of reactions N. Standardized for $E(t) = N/Km_0 = 1$.

The following mathematical treatment is simplified by simulating the profiles in Fig. 6 with $N = 2$ and fitting the time lag of HMWO formation t_M^* and Km_0

$$\frac{M(t)}{M_\infty} = 1 - [1 + Km_0(t - t_M^*)]e^{-Km_0(t-t_M^*)} \quad (6)$$

The fibrils nuclei $N(t)$ are formed after a lag time t_{MN}^* that combines t_M^* with the lag time for the conversion HMWO into nuclei. Due to the significant differences on the timescales of formation of fibrils nuclei by primary and secondary processes, it will be considered that secondary nucleation is spontaneous.

$$\frac{N(t)}{N_\infty} = 1 - [1 + Km_0(t - t_{MN}^*)]e^{-Km_0(t-t_{MN}^*)} \quad (7)$$

N_∞ is the total concentration number of fibrils nuclei formed (either by primary or secondary nucleation), $\alpha m_0/(N+1)$, and α and $(1-\alpha)$ are the fractions of the monomer converted to fibrils nuclei and consumed in fibril elongation, respectively. Assuming that the rate of monomer consumption in fibril elongation is $K_f m(t) N(t)$

$$\frac{m_0 - m(t)}{m_0} = \alpha[1 - (1 + Km_0\tau_M)exp(-Km_0\tau_M)] +$$

$$+(1-\alpha)\left[1 - exp\left[\frac{-K_f\alpha}{K(N+1)}[Km_0\tau_{MN} - 2 + (Km_0\tau_{MN} + 2)exp(-Km_0\tau_{MN})]\right]\right] \quad (8)$$

where $\tau_{MN} = t - t^*_{MN}$ and $\tau_M = t - t^*_M$. Equation 4 is able to simulate the diversity of amyloid kinetic shapes found in the literature (Fig. 7).

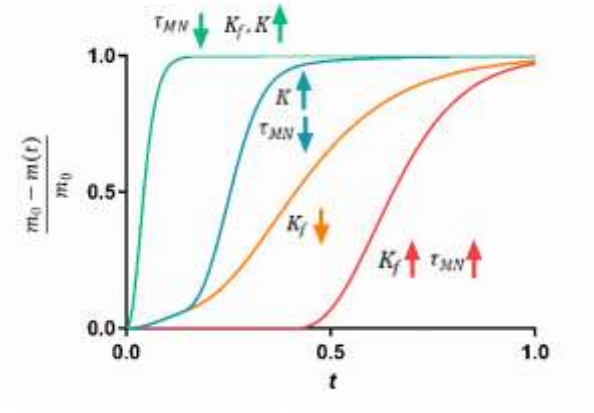

Fig. 7. Amyloid kinetic curve shapes that can be obtained by equation 4.

Aggregation of Aβ1-40 was also monitored by thioflavin-T (ThT) fluorescence. The fibrillation kinetics of Aβ1-40 has been extensively studied by fluorimetric methods; the overall curves have a sigmoidal shape including a lag phase, a growth phase and a plateau. We have obtained the expected sigmoidal curves for Aβ1-40 that can be well reproduced by our

model (Fig 8, top). Moreover, the role that oligomeric species also play in Aβ1-42 aggregation was very recently stressed [28], and thus we decided to apply the model to Aβ1-42 kinetics too (Fig 8, bottom).

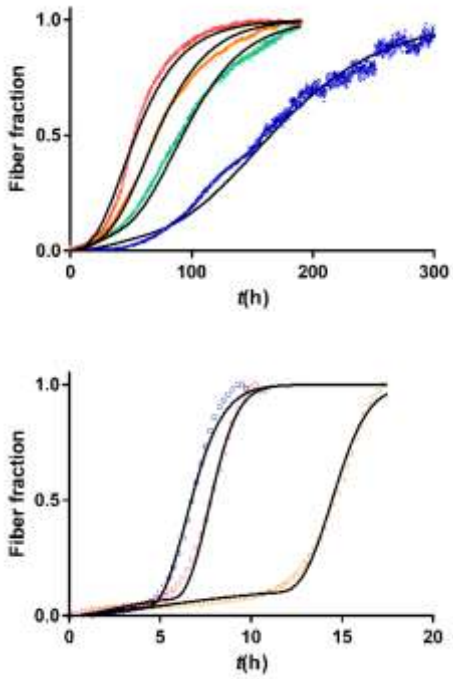

Fig. 8. ThT aggregation kinetic assays of Aβ1-40 (top) and Aβ1-42 (bottom). Initial concentrations of soluble Aβ1-40 are 100, 70, 55 and 30 μM and of Aβ1-42 are 20, 15 and 7.4 μM. Lines represent the best fit obtained with Equation 8.

Despite the very good fitting of the mathematical model to the aggregation kinetics of Aβ1-40 and Aβ1-42, we should stress that we have only investigated the formation of high molecular weight intermediates of Aβ1-40 peptide. Nevertheless, Knowles and colleagues provided evidences that Aβ1-42 mature fibrils must originate from oligomers [28] which supports the application of Equation 8 to the Aβ1-42 kinetic curves.

In conclusion, our findings reveal the role of oligomeric intermediates in the formation of Aβ1-40 amyloid fibrils. Clearly a more systematic investigation is mandatory to fully understand the underlying molecular mechanisms of Aβ1-40 fibrillogenesis but the experimental data displayed here point to the slow formation of high molecular weight oligomers (HMWO) that reorganise structurally into more compact species (nuclei formation) that subsequently proceeds to fibril growth through the addition of soluble Aβ1-40 species. Fibrils nuclei seem to outnumber HMWO which points to a parallel mechanism of nuclei formation, probably heterogeneous nucleation. In addition, the NMR diffusion measurements of Aβ1-40 and Aβ17-40 are consistent with the minority presence of dimers or other small oligomers in solution at the physiological temperature of 37°C.

Acknowledgements

This work was supported by Norte-01-0145-FEDER-000008- Porto Neurosciences and Neurologic Disease Research Initiative at I3S, supported by Norte Portugal Regional Operational Programme (NORTE2020), under the PORTUGAL 2020 Partnership Agreement, by COMPETE 2020—Operacional Programme for Competitiveness and Internationalisation (POCI), Portugal 2020, through the European Regional Development Fund (FEDER), and by Portuguese funds through FCT—Fundação para a Ciência e a Tecnologia/Ministério da Ciência, Tecnologia e Ensino Superior in the framework of the project “Institute for Research and Innovation in Health Sciences” (POCI-01-0145-FEDER-007274) and PhD grant SFRH/BD/129921/2017 (José P. Leite). We also thank Fundacio Marato de TV3 (neurodegenerative diseases call, project reference: 20140330-31-32-33-34). Pablo Taboada thanks the Agencia Estatal de Investigación (AEI) by project MAT2016-80266-R, and Xunta

de Galicia for additional funding (Grupo de Referencia Competitiva ED431C 2018/26 and Agrupación Estratégica en Materiales-AEMAT ED431E 2018/08). ERDF funds are also greatly acknowledged.Ana Gimeno thanks MINECO (Spain) for a Juan de la Cierva contract.

References

[1] T. Mohamed, A. Shakeri, P.P. Rao, Eur J Med Chem, 113 (2016) 258-272.
[2] S.R. Collins, A. Douglass, R.D. Vale, J.S. Weissman, PLoS. Biol., 2 (2004) 1582-1590.
[3] R. Kayed, E. Head, J.L. Thompson, T.M. McIntire, S.C. Milton, C.W. Cotman, C.G. Glabe, Science, 300 (2003) 486-489.
[4] A.M. Morris, M.A. Watzky, R.G. Finke, BBA-Proteins Proteomics, 1794 (2009) 375-397.
[5] C.J. Roberts, Biotechnol. Bioeng., 98 (2007) 927-938.
[6] F. Baftizadeh, X. Biarnes, F. Pietrucci, F. Affinito, A. Laio, J. Am. Chem. Soc., 134 (2012) 3886-3894.
[7] F. Baftizadeh, F. Pietrucci, X. Biarnes, A. Laio, Phys. Rev. Lett., 110 (2013).
[8] R. Cabriolu, D. Kashchiev, S. Auer, J. Chem. Phys., 133 (2010).
[9] R. Crespo, F.A. Rocha, A.M. Damas, P.M. Martins, J. Biol. Chem., 287 (2012) 30585-30594.
[10] F.A. Ferrone, J. Hofrichter, H.R. Sunshine, W.A. Eaton, Biophys. J., 32 (1980) 361-380.
[11] W.F. Xue, S.W. Homans, S.E. Radford, Proc. Natl. Acad. Sci. U. S. A., 105 (2008) 8926-8931.
[12] F. Ferrone, Methods Enzymol., 309 (1999) 256-274.
[13] F.A. Ferrone, J. Hofrichter, W.A. Eaton, Journal of Molecular Biology, 183 (1985) 611-631.
[14] A.M. Morris, M.A. Watzky, J.N. Agar, R.G. Finke, Biochemistry, 47 (2008) 2413-2427.
[15] T.P.J. Knowles, C.A. Waudby, G.L. Devlin, S.I.A. Cohen, A. Aguzzi, M. Vendruscolo, E.M. Terentjev, M.E. Welland, C.M. Dobson, Science, 326 (2009) 1533-1537.
[16] M. Tanaka, S.R. Collins, B.H. Toyama, J.S. Weissman, Nature, 442 (2006) 585-589.
[17] V. Fodera, S. Cataldo, F. Librizzi, B. Pignataro, P. Spiccia, M. Leone, Journal of Physical Chemistry B, 113 (2009) 10830-10837.
[18] R. Jansen, W. Dzwolak, R. Winter, Biophys. J., 88 (2005) 1344-1353.
[19] F. Librizzi, C. Rischel, Protein Science, 14 (2005) 3129-3134.
[20] V. Fodera, M. van de Weert, B. Vestergaard, Soft Matter, 6 (2010) 4413-4419.
[21] A. Lomakin, D.S. Chung, G.B. Benedek, D.A. Kirschner, D.B. Teplow, Proc. Natl. Acad. Sci. U. S. A., 93 (1996) 1125-1129.
[22] S.I.A. Cohen, S. Linse, L.M. Luheshi, E. Hellstrand, D.A. White, L. Rajah, D.E. Otzen, M. Vendruscolo, C.M. Dobson, T.P.J. Knowles, Proc. Natl. Acad. Sci. U. S. A., 110 (2013) 9758-9763.
[23] G. Meisl, X. Yang, E. Hellstrand, B. Frohm, J.B. Kirkegaard, S.I.A. Cohen, C.M. Dobson, S. Linse, T.P.J. Knowles, Proc. Natl. Acad. Sci. U. S. A., 111 (2014) 9384-9389.
[24] G. Bellomo, S. Bologna, L. Gonnelli, E. Ravera, M. Fragai, M. Lelli, C. Luchinat, Chemical Communications, 54 (2018) 7601-7604.
[25] B.R. Sahoo, S.J. Cox, A. Ramamoorthy, Chemical Communications, 56 (2020) 4627-4639.
[26] J.R. Brender, A. Ghosh, S.A. Kotler, J. Krishnamoorthy, S. Bera, V. Morris, T.B. Sil, K. Garai, B. Reif, A. Bhunia, A. Ramamoorthy, Chemical Communications, 55 (2019) 4483-4486.
[27] S.A. Kotler, P. Walsh, J.R. Brender, A. Ramamoorthy, Chemical Society Reviews, 43 (2014) 6692-6700.
[28] T.C.T. Michaels, A. Šarić, S. Curk, K. Bernfur, P. Arosio, G. Meisl, A.J. Dear, S.I.A. Cohen, C.M. Dobson, M. Vendruscolo, S. Linse, T.P.J. Knowles, Nature Chemistry, 12 (2020) 445-451.

[29] K. Broersen, W. Jonckheere, J. Rozenski, A. Vandersteen, K. Pauwels, A. Pastore, F. Rousseau, J. Schymkowitz, Protein Eng Des Sel, 24 (2011) 743-750.
[30] S.B. Stefan Berger, Experiment 11.17 in: Wiley-VCH (Ed.) 200 and More NMR Experiments: A Practical Course, Weinheim, 2004, pp. 509-511.
[31] M. Marquart, J. Walter, J. Deisenhofer, W. Bode, R. Huber, Acta Crystallographica Section B, 39 (1983) 480-490.
[32] A. Ortega, D. Amorós, J. García De La Torre, Biophys. J., 101 (2011) 892-898.
[33] G. Damaschun, H. Damaschun, K. Gast, D. Zirwer, Biochemistry (Moscow), 63 (1998) 259-275.
[34] J. Danielsson, J. Jarvet, P. Damberg, A. Gräslund, Magnetic Resonance in Chemistry, 40 (2002) S89-S97.
[35] D.K. Wilkins, S.B. Grimshaw, V. Receveur, C.M. Dobson, J.A. Jones, L.J. Smith, Biochemistry, 38 (1999) 16424-16431.
[36] M. Lalowski, A. Golabek, C.A. Lemere, D.J. Selkoe, H.M. Wisniewski, R.C. Beavis, B. Frangione, T. Wisniewski, J Biol Chem, 271 (1996) 33623-33631.
[37] N.L. Fawzi, D.S. Libich, J. Ying, V. Tugarinov, G.M. Clore, Angewandte Chemie (International ed. in English), 53 (2014) 10345-10349.
[38] N.L. Fawzi, J. Ying, R. Ghirlando, D.A. Torchia, G.M. Clore, Nature, 480 (2011) 268-272.
[39] S.L. Bernstein, N.F. Dupuis, N.D. Lazo, T. Wyttenbach, M.M. Condron, G. Bitan, D.B. Teplow, J.E. Shea, B.T. Ruotolo, C.V. Robinson, M.T. Bowers, Nature Chemistry, 1 (2009) 326-331.
[40] G. Bitan, M.D. Kirkitadze, A. Lomakin, S.S. Vollers, G.B. Benedek, D.B. Teplow, Proc. Natl. Acad. Sci. U. S. A., 100 (2003) 330-335.
[41] R.C. Bailey, G.S. Eadie, F.H. Schmidt, Biometrics, 30 (1974) 67-75.